Tuning the transition barrier of H_2 dissociation in the hydrogenation of CO_2 to formic acid on Ti-doped Sn_2O_4 clusters†

Plaban J. Sarma,(0000-0002-2457-1559)[a], Dikshita Dowerah[a], Nand K. Gour,(0000-0003-3919-1513)[a], Andrew J. Logsdail,(0000-0002-2277-415X)[b], C. Richard A. Catlow,(0000-0002-1341-1541)[b,c,d] and Ramesh Ch. Deka,(0000-0003-4352-2661)[a,*]

[a]Department of Chemical Sciences, Tezpur University, Tezpur, Assam, India, ramesh@tezu.ernet.in

[b]Cardiff Catalysis Institute, School of Chemistry, Cardiff University, Cardiff CF10 3AT, UK

[c]Department of Chemistry, University College London, 20 Gordon St., London WC1HOAJ, UK

[d]UK Catalysis Hub, Research Complex at Harwell, RAL, Oxford, OX11 0FA, UK

Funding Information

Funder Name :	Science and Engineering Research Board
Funder's main country of origin :	India
Funder ID :	10.13039/501100001843
Award/grant Number :	EMR/2016/003195
Funder Name :	Department of Science and Technology, Ministry of Science and Technology
Funder's main country of origin :	India
Funder ID :	10.13039/501100001409
Award/grant Number :	SR/NM/NS-1147/2016(G)
Funder Name :	Department of Biotechnology, Ministry of Science and Technology
Funder's main country of origin :	India
Funder ID :	10.13039/501100001407
Award/grant Number :	BT/PR16182/NER/ 95/92/2015
Funder Name :	Tezpur University
Funder's main country of origin :	India
Funder ID :	10.13039/501100012624
Award/grant Number :	Unassigned
Funder Name :	UKRI Future Leaders Fellowship
Funder's main country of origin :	UK

Funder ID :
Award/grant Number : MR/T018372/1

Table of Contents Entry

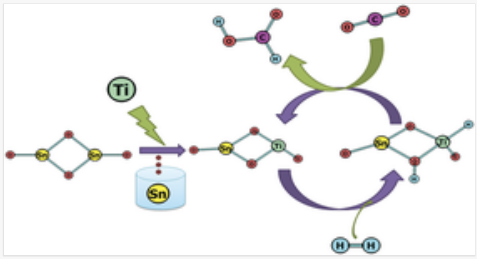

Schematic representation of Ti-doping on a pure Sn_2O_4 cluster for the hydrogenation of CO_2 to HCOOH *via* a hydride pathway.

Abstract

[Instruction: This doesn't really make any sense as written and in the broader context of the abstract. Could it be updated to:
"A density functional theory study has been performed to investigate cation-doped Sn_2O_4 clusters for selective catalytic reduction of CO_2", with the second sentence removed (As this is repeated information below)]~~Titanium-doped Sn_2O_4 clusters show robust catalytic activity for selective CO_2 reduction by~~ A density functional theory study has been performed to investigate cation-doped Sn_2O_4 clusters for selective catalytic reduction of CO_2. ~~Our study focuses on the importance of small-sized clusters in catalytic reduction of CO_2 at a lower overpotential.~~ We ~~investigate~~study the influence of Si and Ti dopants on the height of the H_2 dissociation barrier for~~on~~ the doped systems, and then the subsequent mechanism for the conversion of CO_2 into formic acid (FA) *via* a hydride pinning pathway. The lowest barrier height for H_2 dissociation is observed across the 'Ti–O' bond of the Ti-doped Sn_2O_4 cluster, with a negatively charged hydride (Ti–H) formed during the heterolytic H_2 dissociation, bringing selectivity towards the desired FA product. The formation of a formate intermediate is identified as the rate-determining step (RDS) for the whole pathway, but the barrier height is substantially reduced for the Ti-doped system when compared to the same steps on the undoped Sn_2O_4 cluster. The free energy of formate formation in the RDS is calculated to be negative, which reveals that the hydride transfer would occur spontaneously. Overall, our results show that the small-sized Ti-doped Sn_2O_4 clusters exhibit better catalytic activity than undoped clusters in the important process of reducing CO_2 to FA when proceeding *via* the hydride pinning pathway.

Introduction

Combustion of fossil fuels is a major contributing factor to the increasing atmospheric concentration of CO_2, which is regarded as one of the major anthropogenic contributors to global warming.[1,2] To address the current "Climate Emergency", mitigation of CO_2 either by conversion or trapping is now essential. For this purpose, reduction of CO_2 into commercially valuable chemicals such as formic acid (FA), methanol and longer-chained alcohols is highly advantageous.[3–5] Furthermore, hydrogenation of CO_2 to liquid phase HCOOH and CH_3OH also addresses challenges associated with storage and transport of H_2, with the low volumetric density of H_2 in the gas phase considered prohibitive for its potential use as an energy vector; HCOOH is a non-toxic liquid at room temperature, making it easy to transport and allowing direct implementation in fuel cells.[6] Currently, however, chemical reduction of CO_2 to formic acid is limited by the availability of suitable catalysts to activate the thermodynamically stable C=O bond, which has a bond energy of 5.52 eV (533 kJ mol^{-1}).[7] There are several reported methods of CO_2 reduction, including catalytic hydrogenation, electrochemical reduction, photocatalysis and biological reduction; among these, electrochemical and photochemical reductions are promising for facilitating product selectivity, lower production costs and high catalytic efficiency.[8–10]

During the last decade, the study of Sn-based electrodes for electrochemical CO_2 reduction has grown rapidly due to the higher overpotentials necessary for competing H_2 evolution reactions, thus bringing selectivity to the reduction of CO_2 to HCOOH.[11–13] Like other non-noble metals, tin undergoes corrosion and degradation, but the oxide layer formed has been identified as highly catalytic towards the electrochemical reduction of CO_2. The importance of the oxide layer was highlighted by Chen and Kanan, who reported that the catalytic activity of SnO_2 depends on the oxide layer percentage, showing that the depth of the oxide layer was proportional to the reduction efficiency.[14] Particle sizee ~~effects~~ also has~~ve~~ an important effect on catalyst efficacy, with Xu *et al.* describing the significance of quantum confinement for SnO_2 quantum dots (QDs) within the range of 0.5–2.5 nm, as illustrated for gas sensing properties towards ethanol; QDs show higher sensitivity than larger SnO_2 nanowires.[15] Liu *et al.* compared the electrocatalytic properties of SnO_2 quantum wires (1.7 nm) with SnO_2 nanoparticles (5.5 nm) for HCOOH formation and concluded that the quantum wires have exposed grain boundaries that enhance the current density, as well as faradaic efficiency, by over 80% for HCOOH formation.[16] This also reveals the importance of small-sized clusters in the catalytic reduction of CO_2 to HCOOH and it influences the overpotential of formic acid production.

In contrast to the catalytic application of pure SnO_2 clusters, there is limited literature for the application of doped SnO_2 clusters towards the hydrogenation of CO_2 to HCOOH. H_2 dissociation on doped metal oxide clusters and surfaces such as Al-doped ZnO, CeO_2 and MgO has been reported, as well as on Ni clusters doped with Rh, Pt, Pd and Au metals.[17,18] However, the mechanism of CO_2 reduction using doped-SnO_2 nanoparticles remains relatively unexplored. Saravanan *et al.* performed theoretical calculations of SnO_2 surfaces to try and understand the consequences of transition metal doping,[19] considering two types of dopants: Ti, V, Nb, Ta and Zr replacing the six coordinated Sn(IV) in a pristine crystal; and Cd, Co, Pb, Sb and Zn accompanied by a neighbouring O vacancy, *i.e.* at an Sn(II) site. The extrinsic dopants at the Sn(IV) site resulted in a material showing potential to reduce CO_2 to HCOOH at lower overpotentials than pure SnO_2, with Ti-doped SnO_2 identified as the best catalyst. Such Ti-doped SnO_2 nanoparticles are used currently as sensing materials for ethanol, and both Ti- and Si-doped SnO_2 nanoparticles have been studied to understand the influence of the doping metal on the electrical conductivity.[20–23]

Previously, CO_2 activation on the catalyst surface has been reported as occurring by the formation of a carbonate-like structure, followed by the transfer of a hydrogen atom to the carbon atom, producing formate and subsequently formic acid.[14,23,24] Earlier studies show that H_2 can dissociate heterolytically on ZnO clusters, which leads to the formation of a metal-hydride bond.[17,25] Similarly, another study on SnO_2 reported a hydride pinning pathway whereby heterolytic H_2 dissociation leads to the formation of an Sn-hydride bond, and CO_2 activation occurs during the (rate-determining) hydride transfer step; the observed outcome was total selectivity of HCOOH formation at an overpotential of 0.25 eV.[26] In the present work, we consider whether dopants in a model dimeric Sn_2O_4 cluster modify the key steps in this favourable hydrogenation pathway of CO_2 to HCOOH. Structures for the Sn_2O_4 clusters have been taken from previous studies[26] and, for the newly considered doped system, we chose two dopants: Si, which is isovalent with Sn, with a stable +4 oxidation state as well as vacant 3d orbitals; and Ti, which has an atomic radius similar to Sn, vacant 3d electrons, and stability in the +4 oxidation state (though somewhat reducible). As both dopants are considered formally in +4 oxidation states, their introduction to the cluster does not require compensating oxygen vacancies.

Results and discussion

Structures of Si- and Ti-doped Sn_2O_4 clusters

Si and Ti dopants replace a Sn atom in the small dimeric Sn_2O_4 cluster, and the structures were geometry-optimized using density functional theory (DFT) (Fig. 1). The structure of the $SnSiO_4$ cluster is similar to that of the pure Sn_2O_4 cluster, maintaining a planar 2-dimensional configuration; in contrast, the $SnTiO_4$ cluster is 3-dimensional, with the Ti-center taking a distorted T_d shape surrounded by two bridging and one terminal oxygens. The shape of the TiO_3 unit in the $SnTiO_4$ cluster resembles the Ti-center of a pure Ti_2O_4 cluster.[27]

Fig. 1

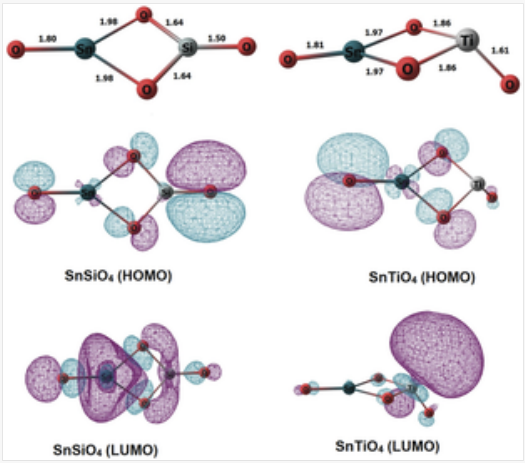

Optimized geometries of $SnSiO_4$ (left) and $SnTiO_4$ (right) clusters, along with the HOMOs and LUMOs, as calculated at the MN12-SX/def2tzvpp level of theory. The different colours (aqua/magenta) of the orbitals indicate the phases of the orbitals taken at the cutoff of 0.03.

The formation energy (E_f) of the doped clusters upon replacement of one Sn by the Si or Ti atom is calculated *via* the equation as follows:

$$E_f = (E_{SnMO_4} + E_{SnO_2}) - (E_{Sn_2O_4} + E_{MO_2}),$$

where M corresponds to the dopant Si or Ti species. The formation energy of the $SnSiO_4$ and $SnTiO_4$ clusters with respect to the Sn_2O_4 and MO_2 (SiO_2 and TiO_2) clusters are calculated to be −0.80 eV (−18.55 kcal mol^{-1}) and −0.73 eV (−16.83 kcal mol^{-1}), respectively, indicating that doping of these small clusters is thermodynamically feasible. $SnSiO_4$ has a lower energy than $SnTiO_4$, due to the greater strength of the Si–O bond.[28]

Natural bond orbital (NBO) calculations have been performed to interpret the bonding interactions of the metal dopants with the oxygen atoms in the clusters, and diagrams of the highest occupied molecular orbitals (HOMOs) and the lowest unoccupied molecular orbitals (LUMOs) are included accordingly in Fig. 1. The HOMOs of both of the doped clusters are concentrated on the lone pairs of oxygen, *i.e.* the non-bonding electrons. The LUMO of $SnSiO_4$ has the π* character of an O–Si bond, and some character of the Sn-center, which provides us the evidence of having an O–Si π interaction resulting from the back donation of electron density from the oxygen lone pairs to the empty 3d orbitals of silicon. To verify the involvement of Si d orbitals in the bonding interactions, we have analyzed the percentage of individual atomic contributions towards the participating bonds in the $SnSiO_4$ and $SnTiO_4$ clusters (Table 1, column 4), along with the orbital contributions of the s, p and d orbitals (Table 1, column 5). Some occupancy of the Si d orbitals is observed in both the terminal and bridging Si–O bonds, along with the s and p orbitals, which reveals that the O–Si π bonding interaction includes the contributions from the Si d orbitals; however, for the $SnTiO_4$ cluster, the percentage contribution of the d orbitals is much more than those of the s and p orbitals. These observations lead us to conclude that the more ~~stable~~ covalent-like Si interactions in the $SnSiO_4$ cluster favourably stabilise the system when compared to those of the Ti-dopant in $SnTiO_4$. The individual atomic contributions (column 4) of the participating bonds show that O contributes significantly to bonding compared to the Sn, Si and Ti atoms.

Table 1

Percentage contribution of orbitals to the bridging and terminal metal-oxygen bonds as calculated *via* an NBO calculation at the MN12-SX/def2TZVPP level of theory

Cluster	Bond type	Atom	Elemental contribution (%)	Angular contribution (%)
$SnSiO_4$	Bridging Si–O	Si	12.65	s (27.98) p (48.21) d (23.78)
		O	87.35	s (33.69) p (65.90)
	Terminal Si–O	Si	19.53	s (43.39) p (55.60) d (0.99)
		O	80.47	s (34.36) p (65.0%)

	Bridging Sn–O	Sn	12.82	s (26.54) p (72.66) d (0.45)
		O	87.18	s (12.24) p (87.36)
	Terminal Sn–O	Sn	29.85	s (46.92) p (52.58) d (0.33)
		O	70.15	s (6.94) p (92.93)
$SnTiO_4$	Bridging Ti–O	Ti	12.86	s (23.60) p (23.94) d (51.79)
		O	87.14	s (29.51) p (70.39)
	Terminal Ti–O	Ti	20.57	s (10.69) p (7.40) d (81.33)
		O	79.43	s (19.70) p (80.22)
	Bridging Sn–O	Sn	13.65	s (27.35) p (71.28) d (0.89)
		O	86.35	s (9.23) p (90.65)
	Terminal Sn–O	Sn	28.95	s (45.08) p (54.31) d (0.43)
		O	71.05	s (7.29) p (92.58)

H_2 dissociation on the $SnMO_4$ clusters

Previously, an undoped Sn_2O_4 cluster~~s~~ has~~ve~~ been observed to dissociate H_2 at Sn–O bridging sites, with the hydride pinning pathway leading to selective reduction of CO_2 to HCOOH *via* a formate intermediate.[26] Considering this observation~~previous work~~, we calculated the transition states and barrier heights of H_2 dissociation on all possible bridging sites in the doped cluster; the subsequent optimized minima and transition state geometries are shown in Fig. 2, and the reaction energy profiles in Fig. 3.

Fig. 2

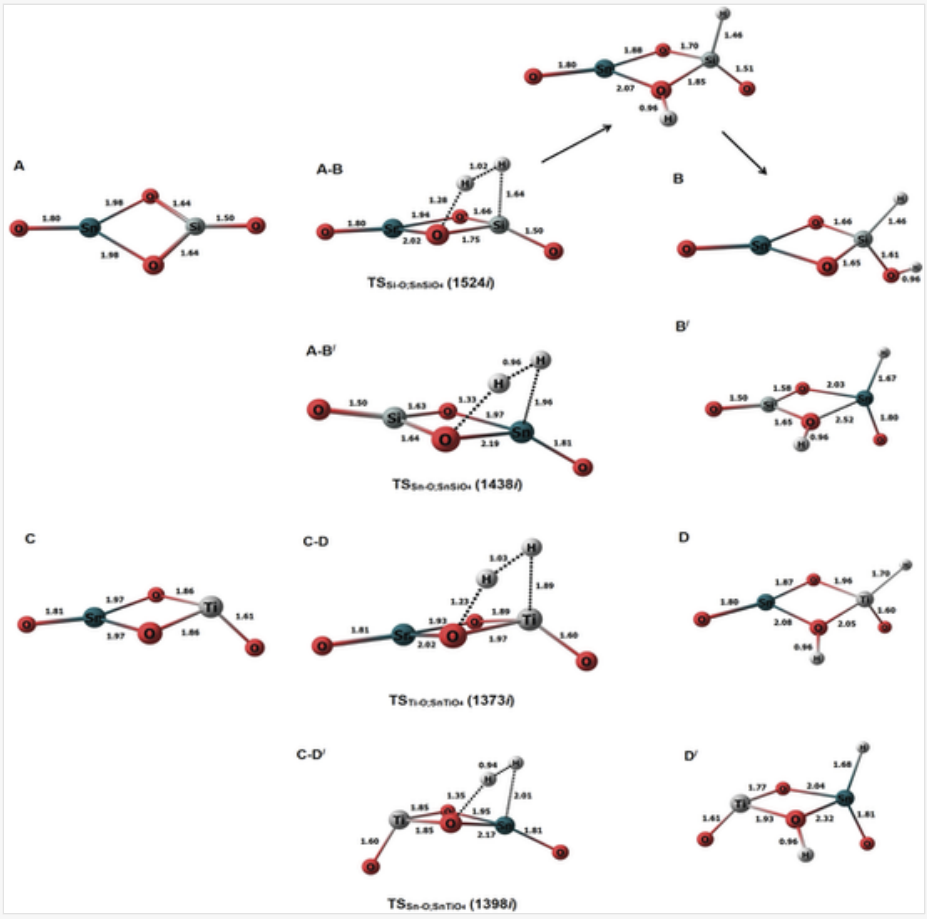

The optimized structures of doped clusters along with the transition states and H_2 dissociated products. Top: $SnSiO_4$; bottom: $SnTiO_4$.

Fig. 3

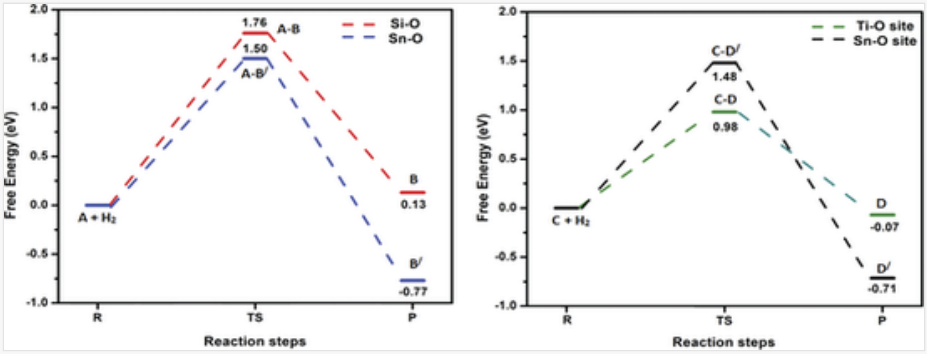

The potential energy profile diagrams comparing the dissociation of H_2 on the 'Sn–O' and 'M–O' sites of the $SnSiO_4$ (left) and $SnTiO_4$ (right) clusters, calculated at the MN12-SX/def2tzvpp level of theory.

For the $SnSiO_4$ cluster, the activation energy for H_2 dissociation is 1.76 eV (40.61 kcal mol^{-1}) on a Si–O bond, which is 0.26 eV (5.99 kcal mol^{-1}) higher than at the Sn–O bond [1.50 eV, 34.73 kcal mol^{-1}]. The transition states corresponding to H_2 dissociation on Si–O (A–B) and Sn–O (A–B′) sites (Fig. 2) are characterized by the presence of imaginary frequencies of 1524*i* cm^{-1} and 1438*i* cm^{-1}, respectively. The dissociated products 'B' and 'B′', formed on the Si–O and Sn–O sites, respectively, are also shown in Fig. 2. Interestingly, despite dissociation occurring at the bridging position of the Si–O site for product B, as confirmed *via* the transition state (A–B) and IRC calculation (Fig. S1, ESI†), the product has a geometry based on the terminal Si–O bond. The convergence graph is shown in Fig. 4 for the reaction A → A–B → B. Fig. 4 indicates that, whilst the H_2 dissociation transition state is at the bridging site, the product H is unstable at this bridging location and converts to a more stable terminal-positioned structure (Fig. 2, structure B). We attribute the formation of the terminal H to the Si–O dπ–pπ interaction observed for the bridging Si–O bond in the $SnSiO_4$ cluster, which provides extra stability to the bridging Si–O bonds; the dπ–pπ interaction is less pronounced in the terminal Si–O bond, with the contribution of the Si d orbital reduced (0.99%, compared to 23.78% for the bridging bond). The H_2 dissociation on the Sn–O site results in similar structural arrangement to H_2 dissociation on the undoped Sn_2O_4 cluster investigated previously.[26]

Fig. 4

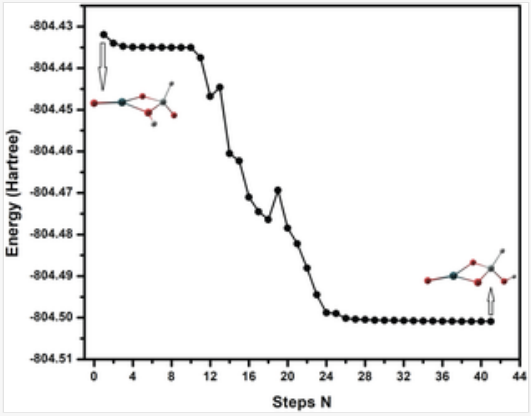

Structural convergence from H_2 dissociation at the bridging 'Si–O' site to terminal 'Si–O' site.

In contrast, the $SnTiO_4$ cluster shows a smaller barrier on the Ti–O bridge (C–D) of 0.98 eV (22.62 kcal mol^{-1}), with an imaginary frequency of 1373*i* cm^{-1}. The barrier height is 0.50 eV (11.68 kcal mol^{-1}) lower than that of the Sn–O bridge (C–D′), as shown in Fig. 3. The lower barrier over the Ti–O bridge can be explained *via* the orbital structures: The LUMO of the $SnTiO_4$ cluster is located on the Ti-center and thus, when H_2 dissociation takes place over the Ti–O bridge, it occurs *via* interaction with the LUMO;; however, on the Sn–O bridge, H_2 dissociation cannot take place

through the Ti-centered LUMO, interacting instead with the LUMO+1 (Fig. S2, ESI†). Therefore, a higher orbital reorganization energy is required for H_2 dissociation over the Sn–O bridge, which leads to a larger activation energy for the process. Notably, H_2 dissociation on the Ti–O site has a lower activation energy than on the Sn–O site in doped and undoped Sn_2O_4 clusters (barrier height = 1.25 eV).[26]

To understand the strength of the M–H bond, and confirm whether the hydride ion has formed, we analyzed the Bader charge of the H_2 dissociated products (B, B′, D and D′) in Table 2. A hydride is observed in all the models, as the hydrogen of newly formed M–H possesses a negative formal charge. The calculated percentages of orbital contributions of H and M in the M–H bond are shown in Table 3; in the bonding of Si–H, the contribution of the Si 3p orbital is the greatest (46.86%), whereas the Ti–H bond is formed most prominently of 3d orbitals (44.90%). In the latter case, the contribution of d is more than those of valence 4s and 4p orbitals, which contribute 25.81% and 29.12%, respectively, and as a consequence the Ti–H bond is weaker than the Si–H bond.

Table 2

Bader charges and bond distances of reacting atoms on all sites of the doped clusters

Structure	Bond	Bond distances, Å	Bader charges, [Instruction: These values cannot be absolute given some are negative!]e
B	Si–H	1.46	Si = +3.15, H = −0.71
	O–H	0.96	O = −1.45, H = +0.70
B′	Sn–H	1.67	Sn = +1.98, H = −0.25
	O–H	0.96	O = −1.53, H = +0.70
D	Ti–H	1.60	Ti = +2.17, H = −0.55
	O–H	0.96	O = −1.37, H = +0.68
D′	Sn–H	1.67	Sn = +1.99, H = −0.27
	O–H	0.96	O = −1.36, H = +0.67

Table 3

Percentage of orbital contribution of all metal-hydride bonds obtained *via* NBO calculation performed at the MN12-SX/def2TZVPP level of theory

Cluster	Atom	Elemental contribution (%)	Angular contribution (%)
$SnSiO_4$	Si	31.60	s (30.85) p (46.86) d (22.21)
	H	68.40	s (99.93) p (0.07)
	Sn	37.57	s (31.12) p (68.44) d (0.33)
	H	62.43	s (99.85) p (0.14)
$SnTiO_4$	Ti	36.88	s (25.81) p (29.12) d (44.90)
	H	63.12	s (99.85) p (0.14)
	Sn	38.10	s (42.59) p (56.78) d (0.56)

	H	61.90	s (99.86) p (0.14)

Mechanistic study *via* hydride pinning pathway

After dissociation of H_2 on the doped Sn_2O_4 cluster, we extended our study to the hydrogenation of CO_2 *via* the hydride pinning pathway. As already discussed, the H_2 dissociation barrier height is lower on $SnTiO_4$ than that on $SnSiO_4$, and hence CO_2 reduction is considered only on the $SnTiO_4$ cluster. The overall pathway follows a two-step catalytic mechanism:[26]

(a) First, gas phase CO_2 takes up the hydride from the catalytic site following the 'Eley Rideal' (ER) mechanism and binds with the Sn-center in the cluster.

(b) Second, the remaining hydrogen transfers to the co-adsorbed oxygen of HCOO by following the 'Langmuir Hinshelwood' (LH) mechanism, to form the product HCOOH.

The potential energy pathway for hydrogenation of CO_2 on the $SnTiO_4$ cluster is presented in Fig. 5. In the mechanism studied, the hydride pinning step is initiated by the product 'D' (Fig. 2) where the hydride is transferred from the Ti-site to the carbon of CO_2 to form the formate (HCOO*) intermediate that further binds with the catalyst by one of the intermediate's oxygens. This hydride transfer step proceeds *via* the transition state TS1 ($607i$ cm^{-1}) to form the intermediate IM2 with an activation energy of 0.49 eV (11.49 kcal mol^{-1}). The transition barrier of the hydride transfer step for~~in~~ the doped system is lower than for the undoped cluster [1.15 eV (26.51 kcal mol^{-1})],[26] which is attributed to two factors: first, the weakness of the Ti–H bond relative to the Sn-H bond, which results in hydride transfer to the carbon being less energetically demanding; second, the Ti-centre in the doped $SnTiO_4$ cluster retains its tetrahedral shape throughout *i.e* energy is not required for structure changes of $SnTiO_4$, unlike for bare Sn_2O_4 where the Sn-centre changes its shape from tetrahedral to planar.[26] In the transition state TS1, the Ti–H bond elongates from 1.60 Å to 1.78 Å, while the bond distances of the newly formed C–H and Sn–O bonds are 1.73 Å and 2.33 Å, respectively. After the formation of the HCOO* intermediate, the orientation spontaneously changes to IM2′ by flipping the –CHO group of HCOO* around the C–O(–Sn) bond, with a ΔG of –0.30 eV (–6.91 kcal mol^{-1}), which then allows uptake of the second hydrogen from the cluster. In the optimized IM2′, we observe a new Sn···O interaction of 2.36 Å (along with the remaining Sn–O bond); the O is now nearer to the remaining H on the cluster, and this hydrogen then transfers from the cluster to form HCOOH. During the formation of HCOOH, IM2′ overcomes an activation barrier of 0.35 eV (8.17 kcal mol^{-1}) *via* the transition state TS2 ($920i$ cm^{-1}), which is smaller than that of the pinning step (TS1) and so indicating that the reaction will proceed rapidly to the equilibrium once the HCOO* intermediate is formed. The HCOOH product leaves the catalytic cycle in the same step and hence the catalyst is recycled for the next H_2 dissociation step.

Fig. 5

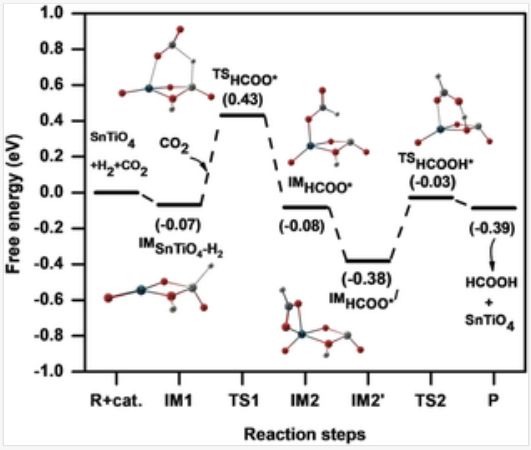

Potential energy diagram representing the hydrogenation of CO_2 to HCOOH on the $SnTiO_4$ cluster *via* the hydride pinning pathway.

For the overall reaction, the hydride pinning step (TS1) is the rate-determining step (RDS) and hence the free energy difference between IM2′ and IM1 equates to the necessary overpotential for realising the hydrogenation process. This

overpotential factor can be calculated from the computational hydrogen electrode (CHE) model given by Nørskov *et al.*,[37] which is discussed in the computational methodology. In the outlined reaction mechanism, the difference in free energies is −0.31 eV, which reveals that the formation of HCOO* intermediate is calculated to be thermodynamically spontaneous. This spontaneity was not observed in the case of undoped Sn_2O_4, where the required overpotential of HCOO* formation is 0.25 eV.[26]

Comparing the present results with previous studies on the hydrogenation of CO_2 to HCOOH on dimeric SnO_2,[26] we can propose the following:

(a) The H_2 dissociation barrier height on the Ti-doped Sn_2O_4 is 0.98 eV, which is 0.54 eV lower than that on the undoped Sn_2O_4 (1.52 eV). The doped cluster is therefore a potentially more active catalyst due to the reduced kinetic H_2 dissociation barrier.

(b) In the hydride transfer step, the barrier height for formate formation is 0.49 eV on the Ti-doped cluster, which is 0.66 eV greater than that on the undoped Sn_2O_4 (1.15 eV). The doped cluster therefore has potentially improved catalytic selectivity towards reduction of CO_2 to HCOOH *via* the hydride pinning pathway.

(c) Lastly, the overpotential factor drops from 0.25 eV when considering~~using~~ the undoped Sn_2O_4 cluster to −0.31 eV for $SnTiO_4$, correlating with the previous work reported by Saravanan *et al.*[19] and illustrating that the reaction would proceed favourably.

Summary and conclusions

Titanium and silicon dopants have been considered on the Sn^{4+} centers of a pure Sn_2O_4 cluster, and subsequently tested in the context of CO_2 hydrogenation. Negative formation energies for $SnSiO_4$ and $SnTiO_4$ reveal the replacement of Sn by Si or Ti to be energetically favourable. H_2 dissociation barrier heights are calculated as favourable on all the bridging sites available on the clusters, with the lowest activation energy on the bridging Ti–O site of the $SnTiO_4$ cluster. Our observations of the potential role for Si and Ti dopants indicates that metals providing π character in the M–O bond will be less suitable catalysts for CO_2 reduction, while first and second row early transition metals (*e.g.* Ti, V, Nb and Zr), are good candidates as dopants in SnO_2 clusters because π bonding is less common. Bader charge analysis of the metal–hydride (Ti–H) shows that one H on each cluster possesses a formal negative charge. The hydride is the key in the hydride-assisted pathways for CO_2 reduction, triggering the total selectivity for the formation of HCOOH over CO at a lower overpotential. The $SnTiO_4$ cluster has a reduced barrier relative to the pure Sn_2O_4 cluster in the rate-determining step (HCOO* formation), and also requires a lower overpotential for the formation of HCOOH, delivering product selectivity. Experimentally, small-sized bare SnO_2 quantum dots are used for the conversion of CO_2 to HCOOH at low overpotentials but the use of Ti-doped SnO_2 particles is not yet reported; therefore, our results should be considered as a stimulus for further experimental investigation of HCOOH formation *via* the hydride pinning pathway.

Methodology

Kohn–Sham density functional theory (DFT), as implemented in the Gaussian 09 software package,[29] has been used to obtain the lowest energy structures and thermochemical properties involved in the mechanism of CO_2 reduction. For geometry relaxation and frequency calculations, a range-separated hybrid non-separable meta-NGA, MN12-SX,[30] is used; the accuracy of the MN12-SX density functional when predicting structures and energies has been extensively studied previously.[26,31,32] A combination of density fitting triple-ξ def2TZVPP basis sets is used,[33] as these minimise the basis set superposition error (BSSE) and give results close to the DFT basis set limit;[34] the BSSE is <0.04 eV with the triple-ξ basis set, and energies reported in the manuscript include this correction.

Frequency calculations are used to confirm the stability of the reactants (Rs), intermediates (IMs) and products (Ps) along the reaction pathway, and to verify the transition states (TSs) identified. The presence of one imaginary frequency, consistent with the eigenvector along with the reaction coordinate, confirms that the TS structure is a first-order saddle point, whereas only real vibrational frequencies are observed for the R, IM and P minima. Changes in the free energy of each reaction step (ΔG) and free energy of activation ($\Delta G^{\ddagger}$) are calculated from the free energy

differences between the final and initial states, assuming room temperature and atmospheric pressure (298 K, 1 atm). Formic acid is formed in the liquid phase at room temperature and therefore, as discussed elsewhere previously, a correction of −0.12 eV (taken from the NIST database) is included in our calculated energy of the FA product to account for the free energy difference between its liquid- and gas-phase forms.[26,35] Bader charge analysis is performed on charge density distribution using the AIMALL software package.[36]

To interpret the overpotential factor associated with the formic acid formation, we have used the computational hydrogen electrode (CHE) model, which correlates the reaction free energy change with the electrochemical potential. We calculate the free energy change at the rate-determining step (RDS), determined as the hydride transfer step to form the HCOO* intermediate, where the CHE gas-phase hydrogen is at equilibrium with a proton and electron pair ($H^+ + e^- \rightarrow 1/2H_2$) at a potential of 0 V against the reversible hydrogen electrode (RHE) for all pH values, all temperatures and 1 atm of pressure.[37]

Conflicts of interest

There are no conflicts to declare.

Acknowledgements

The authors are thankful to the Science & Engineering Research Board (SERB) (EMR/2016/003195), the Department of Science and Technology (DST) nanomission ([SR/NM/NS-1147/2016(G)]) and the Department of Biotechnology (DBT) project (BT/PR16182/NER/95/92/2015) New Delhi, India, and Tezpur University for the financial support. AJL acknowledges funding by the UKRI Future Leaders Fellowship program (MR/T018372/1). The authors gratefully acknowledge Dr Sanjeev P. Mahanta and Dr Dharitri Das of Tezpur University for their valuable suggestions while carrying out the work.

1 J. C. Fyfe, N. P. Gillet and F. W. Zwiers, *Nat. Clim. Change*, 2013, **3**, 767–769.

2 A. Stips, D. Macias, C. Coughlan, E. Garcia-Gorriz and X. S. Liang, *Sci. Rep.*, 2016, **6**, 21691–21699.

3 W. Li, H. Wang, X. Jiang, J. Zhu, Z. Liu, X. Guo and C. Song, *RSC Adv.*, 2018, **8**, 7651–7669.

4 Q. Li, J. Fu, W. Zhu, Z. Chen, B. Shen, L. Wu, Z. Xi, T. Wang, G. Lu, J. Zhu and S. Sun, *J. Am. Chem. Soc.*, 2017, **139**, 4290–4293.

5 A. Álvarez, A. Bansode, A. Urakawa, A. V. Bavykina, T. A. Wezendonk, M. Makkee, J. Gascon and F. Kapteijn, *Chem. Rev.*, 2017, **117**, 9804–9838.

6 A. K. Singh, S. Singh and A. Kumar, *Catal. Sci.*, 2016, **6**, 12–40.

7 K. Ahmad and S. Upadhyayula, *Environ. Prog. Sustainable Energy*, 2019, **38**, 98–111.

8 Z. Sun, T. Ma, H. Tao, Q. Fan and B. Han, *Chem*, 2017, **3**, 560–587.

9 F. Li, L. Chen, G. P. Knowles, D. R. MacFarlane and J. Zhang, *Angew. Chem., Int. Ed.*, 2017, **56**, 505–509.

10 J. Wu, Y. Huang, W. Ye and Y. Li, *Adv. Sci.*, 2017, **4**, 1–29.

11 J. Wu, F. G. Risalvato, S. Ma and X. D. Zhou, *J. Mater. Chem. A*, 2014, **2**, 1647–1651.

12 W. Deng, L. Zhang, L. Li, S. Chen, C. Hu, Z. J. Zhao, T. Wang and J. Gong, *J. Am. Chem. Soc.*, 2019, **141**, 2911–2915.

13 S. Zhang, P. Kang and T. J. Meyer, *J. Am. Chem. Soc.*, 2014, **136**, 1734–1737.

14 Y. Chen and M. W. Kanan, *J. Am. Chem. Soc.*, 2012, **134**, 1986–1989.

15 X. Xu, J. Zhuang and X. Wang, *J. Am. Chem. Soc.*, 2008, **130**, 12527–12535.

16 S. Liu, J. Xiao, X. F. Lu, J. Wang, X. Wang and X. W. Lou, *Angew. Chem., Int. Ed.*, 2019, **58**, 8499–8503.

17 T. W. Keal, P. Sherwood, G. Dutta, A. A. Sokol and C. R. A. Catlow, *Proc. R. Soc. London, Ser. A*, 2011, **467**, 1900–1924.

18 N. S. Venkataramanan, A. Suvitha, H. Mizuseki and Y. Kawazoe, *Int. J. Quantum Chem.*, 2013, **113**, 1940–1948.

19 K. Saravanan, Y. Basdogan, J. Dean and J. A. Keith, *J. Mater. Chem. A*, 2017, **5**, 11756–11763.

20 A. P. S. Isabel, C. H. Kao, R. K. Mahanty, Y. C. S. Wu, C. Y. Li, C. Y. Lin and C. F. Lin, *Ceram. Int.*, 2017, **43**, 10386–10391.

21 J. Q. Wang, H. L. Kang and Y. Zhang, *Mater. Res. Express*, 2018, **5**, 075902–075913.

22 J. Jang, H. Yim and J. W. Choi, *Thin Solid Films*, 2018, **660**, 606–612.

23 Q. Tang, Y. Lee, D. Y. Li, W. Choi, C. W. Liu, D. Lee and D. E. Jiang, *J. Am. Chem. Soc.*, 2017, **139**, 9728–9736.

24 C. W. Lee, N. H. Cho, K. D. Yang and K. T. Nam, *ChemElectroChem*, 2017, **4**, 2130–2136.

25 S. A. French, A. A. Sokol, S. T. Bromley, C. R. A. Catlow, S. C. Rogers, F. King and P. Sherwood, *Angew. Chem., Int. Ed.*, 2001, **40**, 4437–4440.

26 P. J. Sarma, S. D. Baruah, ~~A.~~A. J. Logsdail and R. C. Deka, *ChemPhysChem*, 2019, **20**, 680–686.

27 O. Lamiel-Garcia, A. Cuko, M. Calatayud, F. Illas and S. T. Bromley, *Nanoscale*, 2017, **9**, 1049–1058.

28 F. Weinhold and R. West, *Organometallics*, 2011, **30**, 5815–5824.

29 M. J. Frisch, G. W. Trucks, H. B. Schlegel, G. E. Scuseria, M. A. Robb, J. R. Cheeseman, G. Scalmani, V. Barone, B. Mennucci and G. A. Petersson, *et al.*, Gaussian09 Revision D.01, Gaussian Inc., Wallingford CT. 2010

30 R. Peverati and D. G. Truhlar, *Phys. Chem. Chem. Phys.*, 2012, **14**, 16187–16191.

31 F. Weigend, *Phys. Chem. Chem. Phys.*, 2006, **8**, 1057–1065.

32 F. Weigend and R. Ahlrichs, *Phys. Chem. Chem. Phys.*, 2005, **7**, 3297–3305.

33 J. Frau and D. Glossman-Mitnik, *Theor. Chem. Acc.*, 2018, **137**, 1–10.

34 S. Paranthaman, J. Moon, J. Kim, D. E. Kim and T. K. Kim, *J. Phys. Chem. A*, 2016, **120**, 2128–2134.

35 H. Afeefy, J. Liebman and S. Stein, Neutral thermochemical data. in ed. P. Linstrom and W. Mallard, NIST Chemistry WebBook, NIST Standard Reference Database Number. 69 (National Institute of Standards and Technology), Gaithersburg MD, USA, 2010

36 AIMAll (Version 17.11.14), Todd A. Keith, TK Gristmill Software, Overland Park KS, USA, 2017 (aim.tk gristmill.com)

37 J. K. Nørskov, J. Rossmeisl, A. Logadottir, L. Lindqvist, J. R. Kitchin, T. Bligaard and H. Jónsson, *J. Phys. Chem. B*, 2004, **108**, 17886–17892.

Footnotes

[†] Electronic supplementary information (ESI) available. See DOI: 10.1039/d0cp04472e

Queries and Answers

Q1

Query: Funder details have been incorporated in the funder table using information provided in the article text. Please check that the funder information in the table is correct.

Answer: Yes, all informations are correct.

Q2

Query: For your information: You can cite this article before you receive notification of the page numbers by using the following format: (authors), Phys. Chem. Chem. Phys., (year), DOI: 10.1039/d0cp04472e.

Answer: Thank you

Q3

Query: Have all of the author names been spelled and formatted correctly? Names will be indexed and cited as shown on the proof, so these must be correct. No late corrections can be made.

Answer: Yes

Q4

Query: Have all of the funders of your work been fully and accurately acknowledged?

Answer: Yes

Q5

Query: Ref. 6: Please provide the initial(s) for the 3rd author.

Answer: Added successfully